

A QoS-aware Underwater Optimization Framework for Inter-vehicle Communication using Acoustic Directional Transducers

Baozhi Chen and Dario Pompili, *Senior Member, IEEE*

Abstract—Underwater acoustic communications consume a significant amount of energy due to the high transmission power (10 – 50 W) and long data packet transmission times (0.1 – 1 s). Mobile Autonomous Underwater Vehicles (AUVs) can conserve energy by waiting for the ‘best’ network topology configuration, e.g., a *favorable alignment*, before starting to communicate. Due to the frequency-selective underwater acoustic ambient noise and high medium power absorption – which increases exponentially with distance – a shorter distance between AUVs translates into a lower transmission loss and a higher available bandwidth. By leveraging the predictability of AUV trajectories, a novel solution is proposed that optimizes communications by delaying packet transmissions in order to wait for a favorable network topology (thus trading end-to-end delay for energy and/or throughput). In addition, the solution proposed – which is implemented and compared with geographic routing solutions and delay-tolerant networking solutions using an emulator that integrates underwater acoustic WHOI Micro-Modems – exploits the frequency-dependent radiation pattern of underwater acoustic transducers to reduce communication energy consumption by adjusting the transducer directivity on the fly.

Index Terms—Underwater acoustic sensor networks, autonomous underwater vehicles, position uncertainty.

I. INTRODUCTION

UNDERWATER Acoustic Sensor Networks (UW-ASNs) [2] have been deployed to carry out collaborative monitoring tasks including oceanographic data collection, disaster prevention, and navigation. To enable advanced underwater explorations, Autonomous Underwater Vehicles (AUVs), equipped with underwater sensors, are used for information gathering. Underwater *gliders* are one type of battery-powered energy-efficient AUVs that use hydraulic pumps to vary their volume in order to generate the buoyancy changes that power their forward gliding. These gliders are designed to rely on local intelligence with minimal onshore operator dependence. Acoustic communication technology is employed to transfer vital information (data and configuration) among gliders

Manuscript received July 5, 2013; accepted January 5, 2014. The associate editor coordinating the review of this paper and approving it for publication was M.-O. Pun.

A preliminary shorter version of this paper is in Proc. of *IEEE Conference on Sensor, Mesh and Ad Hoc Communications and Networks (SECON)*, Salt Lake City, UT, June 2011 [1]. With respect to the conference version, the current manuscript has been substantially extended and revised.

This work was supported by the NSF CAREER Award No. OCI-1054234. The authors are with Department of Electrical and Computer Engineering, Rutgers University, New Brunswick, NJ (e-mails: baozhi_chen@cac.rutgers.edu, pompili@ece.rutgers.edu).

Digital Object Identifier 10.1109/TWC.2013.131203

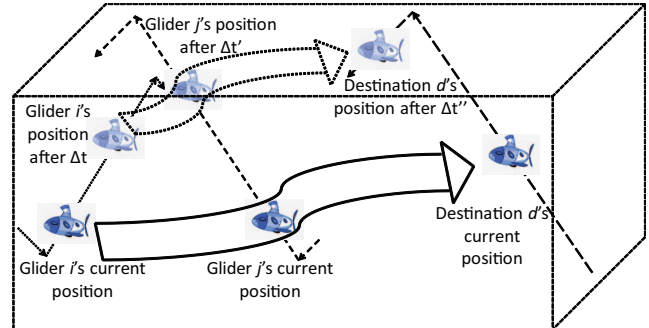


Fig. 1. Glider i delays its transmission by Δt waiting for a better topology so to improve the end-to-end (e2e) energy and/or throughput to destination d . Wide arrows represent the packet forwarding routes and dashed/dotted simple arrows represent glider trajectories.

underwater and, ultimately, to a surface station where this information is gathered and analyzed.

Position information is of vital importance in mobile underwater sensor networks as the data collected has to be associated with appropriate location in order to be spatially reconstructed onshore. Even though AUVs can surface periodically (e.g., every few hours) to locate themselves using Global Positioning System (GPS) – which does not work underwater – over time inaccuracies in models for deriving position estimates, self-localization errors, and drifting due to ocean currents will significantly increase the uncertainty in position of underwater vehicle. Such uncertainty may degrade the quality of collected data and also the efficiency, reliability, and data rates of underwater inter-vehicle communications [3]. Besides the need to associate sensor data with 3D positions, position information can also be helpful for underwater communications. For example, underwater geographic routing protocols (e.g., [4], [5]) assume the positions of the nodes are known. AUVs involved in exploratory missions usually follow predictable trajectories, e.g., gliders follow *sawtooth* trajectories, which can be used to predict position and, therefore, to improve communication.

By leveraging the predictability of the AUVs' trajectory, the energy consumption for communication can be minimized by delaying packet transmissions in order to wait for a *favorable network topology*, thus trading end-to-end (e2e) delay for en-

ergy and/or throughput¹. For instance, Fig. 1 depicts a scenario where glider i waits for a certain time period Δt [s] to save transmission energy and to achieve higher throughput. Based on j 's and d 's trajectory, glider i predicts a ‘better’ topology with shorter links after Δt and postpones transmission in favor of lower transmission energy and higher data rate. This approach differs from that proposed for Delay Tolerant Networks (DTNs), where delaying transmission becomes necessary to overcome the temporary lack of network connectivity [7].

To estimate an AUV's position, in [8] we proposed a statistical approach to estimate a glider's trajectory. The estimates were used to minimize e2e energy consumption for networks where packets in the queue need to be forwarded right away (delay-sensitive traffic). In this work, we focus on delay-tolerant traffic and propose an optimization framework that uses acoustic directional transducers to reduce the computation and communication overhead for inter-vehicle data transmission. Moreover, we offer the distinction between two forms of position uncertainty depending on the network point of view, i.e., *internal* and *external uncertainty*, which refer to the position uncertainty associated with a particular entity/node (such as an AUV) as seen *by itself* or *by others*, respectively (see Sect. IV-A for more details).

Based on the estimated external uncertainty, we propose QUO VADIS², a **Q**oS-aware **u**nderwater **o**ptimization framework for inter-vehicle communication using **a**coustic **d**irectional transducers. QUO VADIS is a cross-layer optimization framework for delay-tolerant UW-ASNs that jointly considers the e2e delay requirements and constraints of underwater acoustic communication modems, including transducer directivity, power control, packet length, modulation, and coding schemes. Specifically, the proposed framework uses the external-uncertainty region estimates of the gliders and forwards delay-tolerant traffic with large maximum e2e delay, which includes *Class I (delay-tolerant, loss-tolerant)* traffic and *Class II (delay-tolerant, loss-sensitive)* traffic [5]. Moreover, our cross-layer communication framework exploits the frequency-dependent radiation pattern of underwater acoustic transducers. By decreasing the frequency band, transducers can change their “directivity” turning from being almost omnidirectional (with a gain of ≈ 0 dBi) – which is a desirable feature to support neighbor discovery and multicasting, geocasting, anycasting, and broadcasting) – to directional (with gains up to 10 dBi) – which is useful for long-haul unicast transmissions.

The contributions of this work are as follows:

- We offer the distinction between two forms of position uncertainty (internal and external, depending on the view of the different nodes). A statistical approach is then proposed to estimate the position uncertainty and this estimated uncertainty is then used to improve network performance.
- We exploit the frequency-dependent directivity of the acoustic transducer that is originally used as omnidirec-

tional transducer at one frequency to optimize network performance.

- We propose a distributed communication framework for delay-tolerant applications where AUVs can conserve energy by waiting for a ‘good’ network topology configuration, e.g., a *favorable alignment*, before starting to communicate.

The remainder of this article is organized as follows. We first review the related work in Sect. II. Then we present the underwater communication model in Sect. III and propose our solution, QUO VADIS, in Sect. IV. In Sect. V, performance evaluation and analysis are carried out, while conclusions are discussed in Sect. VI.

II. RELATED WORK

We review the following areas: geographical routing solutions, terrestrial and underwater DTN solutions, solutions using directional transducers and underwater cross-layer optimization solutions, which are related to our work.

Geographic routing protocols rely on geographic position information for message forwarding, which requires that each node can determine its own location and that the source is aware of the location of the destination. Many geographical routing schemes, including some well-known ones such as Most Forward within Radius (MFR) scheme [9], Greedy Routing Scheme (GRS) [10] and Compass Routing Method (CRM) [11], have been proposed for terrestrial wireless networks. In MFR, the message is forwarded to the neighbor that is closest to the destination, while in GRS a node selects the neighbor whose projection on the segment from the source to destination is closest to the destination. In the CRM [11], a message is forwarded to a neighbor whose direction from the transmitter is the closest to the direction to the destination. In [12], a scheme called Partial Topology Knowledge Forwarding (PTKF) is introduced, and is shown to outperform other existing schemes in typical application scenarios. Based on the estimate using local neighborhood information, PTKF forwards packet to the neighbor that has the minimal e2e routing energy consumption. These solutions are proposed for terrestrial wireless networks. In UW-ASNs, they may not work well since propagation of acoustic signals is quite different from that of radio signals. Moreover, localization underwater is generally more difficult than in the terrestrial environment.

Solutions for DTNs have been proposed for communications within extreme and performance-challenged environments where continuous e2e connectivity does not hold most of the time [7], [13]. Many approaches such as Resource Allocation Protocol for Intentional DTN (RAPID) routing [14], Spray and Wait [15], and MaxProp [16], are solutions mainly for intermittently connected terrestrial networks. RAPID [14] translates the e2e routing metric requirement such as minimizing average delay, minimizing worst-case delay, and maximizing the number of packets delivered before a deadline into per-packet utilities. At a transfer opportunity, it replicates a packet that locally results in the highest increase in utility. Spray and Wait [15] “sprays” a number of copies per packet into the network, and then “waits” until one of these nodes meets the destination. In this way it balances the tradeoff

¹Due to the peculiar ‘V’ shape of the underwater acoustic ambient noise and the high medium power absorption exponentially increasing with distance [6], a shorter distance between AUVs translates into a lower transmission loss and a higher available bandwidth.

²“Quo vadis?” is a Latin phrase meaning “Where are you going?”.

between the energy consumption incurred by flooding-based routing schemes and the delay incurred by spraying only one copy per packet in one transmission. MaxProp [16] prioritizes both the schedule of packets transmissions and the schedule of packets to be dropped, based on the path likelihoods to peers estimated from historical data and complementary mechanisms including acknowledgments, a head-start for new packets, and lists of previous intermediaries. It is shown that MaxProp performs better than protocols that know the meeting schedule between peers. These terrestrial DTN solutions may not achieve the optimal performance underwater as the characteristics of underwater communications are not considered. Hence, in the rest of this section, we focus on related solutions for UW-ASNs.

Several DTN solutions for UW-ASNs have been proposed in [17]–[20]. In [17], an energy-efficient protocol is proposed for delay-tolerant data-retrieval applications. Efficient erasure codes and Low Density Parity Check (LDPC) codes are also used to reduce Packet Error Rate (PER) in the underwater environment. In [18], an adaptive routing algorithm exploiting message redundancy and resource reallocation is proposed so that ‘more important’ packets can obtain more resources than other packets. Simulation results showed that this approach can provide differentiated packet delivery according to application requirements and can achieve a good e2e performance trade-off among delivery ratio, average e2e delay, and energy consumption. A Prediction Assisted Single-copy Routing (PASR) scheme that can be instantiated for different mobility models is proposed in [19]. An effective greedy algorithm is adopted to capture the features of network mobility patterns and to provide guidance on how to use historical information. It is shown that the proposed scheme is energy efficient and cognizant of the underlying mobility patterns.

In [20], an approach called Delay-tolerant Data Dolphin (DDD) is proposed to exploit the mobility of a small number of capable collector nodes (namely dolphins) to harvest information sensed by low power sensor devices while saving sensor battery power. DDD performs only one-hop transmissions to avoid energy-costly multi-hop relaying. Simulation results showed that limited numbers of dolphins can achieve good data-collection requirements in most application scenarios. However, data collection may take a long time as the nodes need to wait until a dolphin moves into the communication ranges of these nodes.

Compared to the number of approaches using directional antennae for terrestrial wireless sensor networks, solutions using directional transducers for UW-ASNs are very limited due to the complexity of estimating position and direction of vehicles underwater. Moreover, these solutions generally assume the transducers are ideally directional, i.e., they assume the radiation energy of the transducer is focused on some angle range with no leaking of radiation energy outside this range. For example, such transducers are used for localization using directional beacons in [21] and for directional packet forwarding in [22]. These solutions also use only one frequency. In our work, rather than using the ideal transducer model, we consider the radiation patterns of existing real-world transducers at different frequencies in order to minimize energy consumption for communications.

A cross-layer optimization solution for UW-ASNs has been proposed in [5], where the interaction between routing functions and underwater characteristics is exploited, resulting in improvement in e2e network performance in terms of energy and throughput. Another cross-layer approach that improves energy consumption performance by jointly considering routing, MAC, and physical layer functionalities is proposed in [4]. These solutions, however, do not consider uncertainty in the AUV positions and are implemented and tested only by software simulation platforms and are not designed for delay-tolerant applications. On the contrary, we propose a practical uncertainty-aware cross-layer solution that incorporates the functionalities of the WHOI Micro-Modem [23] to minimize energy consumption. Moreover, our solution is implemented on real hardware and tested in our emulator integrating WHOI underwater acoustic modems.

III. NETWORK MODEL

In this section we introduce the network model that our solution is based on and state the related assumptions. Suppose the network is composed of a number of gliders, which are deployed in the ocean for long periods of time (weeks or months) to collect oceanographic data. For propulsion, they change their buoyancy using a pump and use lift on wings to convert vertical velocity into forward motion as they rise and fall through the ocean. They travel at a fairly constant horizontal speed, typically 0.25 m/s [2]. Gliders control their heading toward predefined waypoints using a magnetic compass.

Assume the gliders need to forward the data they sensed to a collecting glider. The slow-varying and mission-dependent (and, for such reasons, ‘predictable’) trajectory of a glider is used in our solution to estimate another glider’s position using the position and velocity estimate from some time earlier. A glider estimates its own trajectory and position uncertainty using its own position estimates; the parameters of the estimated trajectory and internal-uncertainty region are sent to neighboring gliders. Using these parameters, these gliders can extrapolate the glider’s current position and a confidence region accounting for possible deviation from the extrapolated course.

The Urick model is used to estimate the transmission loss $TL(l, f)$ [dB] as,

$$TL(l, f) = \kappa \cdot 10 \log_{10}(l) + \alpha(f) \cdot l, \quad (1)$$

where l [m] is the distance between the transmitter and receiver, and f [Hz] is the carrier frequency. Spreading factor κ is taken to be 1.5 for practical spreading, and $\alpha(f)$ [dB/m] represents an absorption coefficient that increases with f [6].

The Urick model is a coarse approximation for underwater acoustic wave transmission loss. In reality, sound propagation speed varies with water temperature, salinity, and pressure, which causes wave paths to bend. Acoustic waves are also reflected from the surface and bottom. Such uneven propagation of waves results in *convergence (or shadow) zones*, which are characterized by lower (or higher) transmission loss than that predicted by the Urick model due to the uneven energy dispersion.

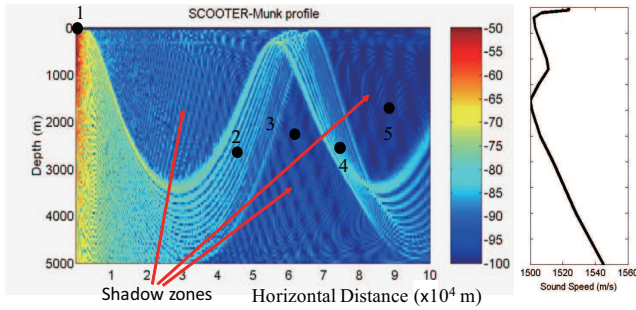


Fig. 2. Shadow zone scenario: the left subfigure represents the transmission loss of node 1 located at the origin, while the right subfigure depicts the sound speed profile used to derive the transmission loss (the y -axis is the depth, which has the same range used in the left; the blue, yellow and red areas denote large, medium and small path losses, respectively)

Due to these phenomena, the Urick model is not sufficient to describe the underwater channel for simulation purposes. The Bellhop model is based on ray/beam tracing, which can model these phenomena more accurately. This model can estimate the transmission loss by two-dimensional acoustic ray tracing for a given sound-speed depth profile or field, in ocean waveguides with flat or variable absorbing boundaries. Transmission loss is calculated by solving differential ray equations, and a numerical solution is provided by HLS Research [24]. Bellhop performs two-dimensional acoustic ray tracing for a given sound speed profile (or sound speed field), in ocean waveguides with flat or variable absorbing boundaries, and generates output such as transmission loss and amplitude based on the theory of Gaussian beams [25]. Due to space limitation, we cannot give a detailed description, but more details can be found in [26].

An example plotted using the Bellhop model is shown in Fig. 2. Interesting enough, if node 1 sends a packet, node 4 has higher probability of receiving the packet than node 3 even though this node is closer. Because the Bellhop model requires more information about the environment than a glider will have, such as sound speed profile of the whole 3D region and depths of receivers and ocean boundary, it is only used to simulate the acoustic environment for testing (relying on trace files with historic data). Hence, the proposed solution uses the Urick model in the cross-layer optimization (Sect. IV-B), which can be computed online on the glider.

We adopt the empirical ambient noise model presented in [6], where a ‘V’ structure of the power spectrum density (psd) is shown. The ambient noise power is obtained by integrating the empirical psd over the frequency band in use³.

IV. PROPOSED APPROACH

Our proposed optimization is based on the estimation of the gliders’ trajectories and their external-uncertainty regions. Therefore, in this section, we introduce the estimation of external-uncertainty regions for gliders first. We then present the cross-layer design of our proposed framework.

³Note that in underwater acoustics, power (or source level) is usually expressed using decibel (dB) scale, relative to the reference pressure level in underwater acoustics $1\mu Pa$, i.e., the power induced by $1\mu Pa$ pressure. The conversion expression for the source level SL re μPa at the distance of 1 m of a compact source of P watts is $SL = 170.77 + 10 \log_{10} P$.

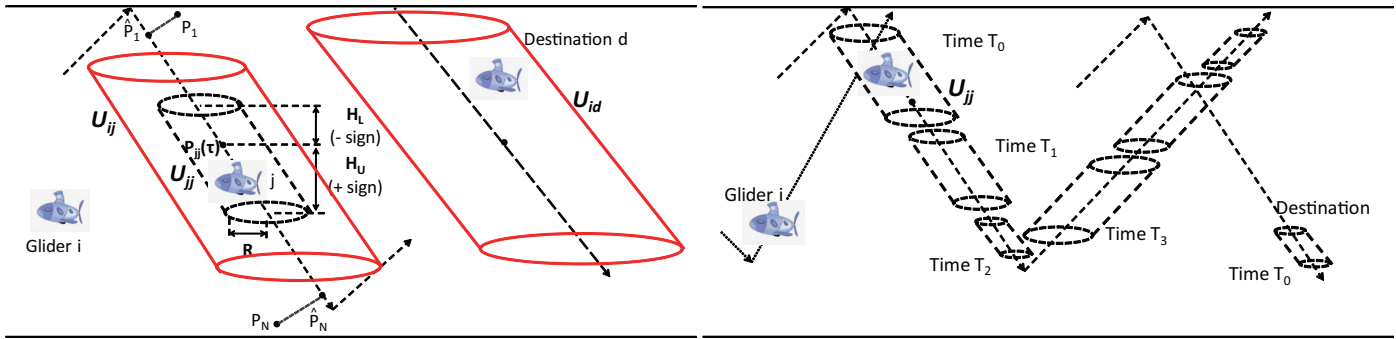
A. Internal and External Uncertainty

When an AUV surfaces to synch with the GPS satellites and obtain its updated position, energy is spent and time is wasted (not to mention the risk that – as it has happened – the vehicle is stolen by pirates or damaged by vandals). In some applications such as coastal tactical surveillance, it is necessary not to surface or rely on surface vehicle. For these reasons, in order to maximize the success probability of a collaborative mission (and/or to minimize its duration), AUVs need to surface only when strictly needed or required by the mission itself. Another way to estimate an AUV’s location is to rely on nodes or vehicles (autonomous or not) with accurate position and use them as reference nodes for localization. Based on these reference locations, the AUV applies localization algorithms such as range-based ones (e.g., [27]) to estimate its own location. Some solutions such as [28], [29] are proposed to use a surface vehicle with accurate GPS information to localize a vehicle underwater, which still requires a vehicle to stay on the surface. In this work we aim at keeping the surfacing of mobile AUVs minimal without using surface vehicles. Under such constraints, we propose algorithms to estimate the AUV’s position and associated uncertainty, and we further use the estimate of position and uncertainty to optimize inter-vehicle communications.

In this subsection, we first offer the distinction between two types of position uncertainty, followed by the discussion on the relationship between these two types of uncertainty. Then we present the statistical approach for external-uncertainty estimation when gliders are used as AUVs and ocean currents are unknown. Since the details have been presented in [1], we just summarize them here.

Internal uncertainty refers to the position uncertainty associated with a particular entity/node (such as an AUV) *as seen by itself*. Existing approaches such as those using Kalman Filter (KF) [30] may not guarantee the optimality when the linearity assumption between variables does not hold. On the other hand, approaches using non-linear filters such as the extended or unscented KF attempt to minimize the mean squared errors in estimates by jointly considering the navigation location and the sensed states/features such as underwater terrain features, which are non-trivial, especially in an unstructured underwater environment.

External uncertainty, as introduced in this work, refers to the position uncertainty associated with a particular entity/node *as seen by others*. Let us denote the internal uncertainty, a 3D region associated with any node $j \in \mathcal{N}$ (\mathcal{N} is the set of network nodes), as \mathcal{U}_{jj} , and the external uncertainties, 3D regions associated with j as seen by $i, k \in \mathcal{N}$, as \mathcal{U}_{ij} and \mathcal{U}_{kj} , respectively ($i \neq j \neq k$). In general, \mathcal{U}_{jj} , \mathcal{U}_{ij} , and \mathcal{U}_{kj} are different from each other; also, due to asymmetry, \mathcal{U}_{ij} is in general different from \mathcal{U}_{ji} . External uncertainties may be derived from the broadcast/propagated internal-uncertainty estimates (e.g., using *one-hop or multi-hop neighbor discovery mechanisms*) and, hence, will be affected by *e2e network latency and information loss*.



(a) Estimated internal-uncertainty region by j : a cylinder with circular bottom radius R and height $H_U - H_L$

(b) Change of internal-uncertainty region over time.

Fig. 3. External- and internal-uncertainty regions for gliders under the effect of unknown ocean currents.

The estimation of the external-uncertainty region⁴ \mathcal{U}_{ij} of a generic node j at node i (with $i \neq j$) involves the participation of both i and j . Here we use the received \mathcal{U}_{jj} as \mathcal{U}_{ij} (a delayed version due to propagation delay, transmission delay, and packet loss). Better estimation of \mathcal{U}_{ij} involves estimation of the change of \mathcal{U}_{jj} with time and is left as future work. We provide a solution for internal- and external-uncertainty estimation when 1) *gliders are used* (following a ‘sawtooth’ trajectory) and 2) *ocean currents are unknown*.

Internal-uncertainty estimation at j : Assume gliders estimate their own locations over time using *dead reckoning*. Given glider j ’s estimated coordinates, $P_n = (x_n, y_n, z_n)$ at sampling times t_n ($n = 1 \dots N$), as shown in [1], its trajectory segment can be described as $P(t) = \bar{P} + \vec{v}(t - \bar{t})$, where $\bar{P} = (\bar{x}, \bar{y}, \bar{z}) = \frac{1}{N} \sum_{n=1}^N (x_n, y_n, z_n)$ and $\vec{v} = \frac{\|\bar{P}_1 \bar{P}_N\|}{\|(a^*, b^*, c^*) \cdot (t_N - t_1)\|} \cdot (a^*, b^*, c^*)$. Here, $[a^*, b^*, c^*]^T$ is the singular vector of $N \times 3$ matrix $\mathbf{A} = [[x_1 - \bar{x}, \dots, x_N - \bar{x}], [y_1 - \bar{y}, \dots, y_N - \bar{y}], [z_1 - \bar{z}, \dots, z_N - \bar{z}]]^T$ corresponding to its largest absolute singular value, $\bar{t} = \frac{1}{N} \sum_{n=1}^N t_n$ is the average of the sampling times, and \bar{P}_i is the projection of point P_i on the line segment (Fig. 3(a)).

The internal-uncertainty region of j is estimated as a *cylindrical* region [1] \mathcal{U} described by its radius R and its height $H_U - H_L$, where H_U and H_L – in general different – are the *signed distances* of the cylinder’s top and bottom surface (i.e., the surface ahead and behind in the trajectory direction, respectively) to glider j ’s expected location on the trajectory. In [8] we demonstrate that:

1) H_L and H_U can be estimated as

$$\begin{cases} H_L = \bar{H} - \hat{t}_{\alpha, N-1} S^{(H)} \sqrt{1 + 1/N} \\ H_U = \bar{H} + \hat{t}_{\alpha, N-1} S^{(H)} \sqrt{1 + 1/N} \end{cases}, \quad (2)$$

where $\bar{H} = \sum_{n=1}^N H_n / N$ is the mean of these N samples, $S^{(H)} = [\frac{1}{N-1} \sum_{n=1}^N (H_n - \bar{H})^2]^{1/2}$ is the unbiased standard deviation, $1 - \alpha$ is the confidence level, and $\hat{t}_{\alpha, N-1}$ is the 100(1 - $\alpha/2$)% of *Student’s t-distribution* [31] with $N - 1$

⁴Note that, ‘‘internal uncertainty’’ is essentially the position probability distribution (with corresponding distribution region) sensed by the vehicle itself, and ‘‘external uncertainty’’ is essentially the position probability distribution (with corresponding distribution region) sensed by other vehicles. For simplicity, we also use ‘‘uncertainty region’’ to represent the probability distribution and the corresponding region where the AUV is distributed for a given confidence level.

degrees of freedom (here H_n is the n -th sample calculated from P_n ’s [8]); and

2) R is estimated by

$$R = \frac{\sqrt{N-1} S^{(R)}}{\sqrt{\hat{\chi}_{\alpha, 2(N-1)}}}, \quad (3)$$

where $S^{(R)} = [\frac{1}{N-1} \sum_{n=1}^N (R_n - \bar{R})^2]^{1/2}$, $\bar{R} = \frac{1}{N} \sum_{n=1}^N R_n$, and $\hat{\chi}_{\alpha, 2(N-1)}$ is the 100(1 - α)% of χ -distribution with $2(N - 1)$ degrees of freedom (here R_n is the n -th sample calculated from P_n ’s [8]). As shown in Fig. 3(b), j ’s internal-uncertainty region becomes smaller over time (from T_0 to T_2), i.e., as more position estimates are acquired. Note that parameter α in the above expressions gives the error probability of the uncertainty estimate and the impact of estimate error will be evaluated in Sect. V.

External-uncertainty estimation at i : After receiving j ’s trajectory and internal-uncertainty region parameters ($\bar{P}, \bar{t}, \vec{v}, H_U, H_L, R$), glider i can update the estimate of j ’s external-uncertainty region. Because AUVs involved in missions show predictable trajectories, information about the sawtooth segment can be used to derive the entire glider trajectory through extrapolation assuming symmetry between glider ascent and descent. Due to packet delays and losses in the network, j ’s external-uncertainty regions as seen by single- and multi-hop neighbors are *delayed versions* of j ’s own internal uncertainty (Fig. 3(b)). Hence, when using *multi-hop neighbor discovery schemes*, the internal uncertainty of a generic node j , \mathcal{U}_{jj} , provides a *lower bound* for all the external uncertainties associated with that node, $\mathcal{U}_{ij}, \forall i \in \mathcal{N}$. Hence we use the received \mathcal{U}_{jj} as \mathcal{U}_{ij} (a delayed version due to propagation delay, transmission delay, and packet loss).

B. Cross-layer Optimization for Delay-tolerant Applications

With the external-uncertainty regions, a glider needs to select an appropriate neighbor to forward each packet to its final destination. Because the major part of available energy in battery-powered gliders is generally devoted to propulsion, acoustic communications should not take a large portion of the available energy. Our proposed protocol minimizes the energy spent to send a message to its destination and considers the functionalities of a real acoustic modem for a practical solution. Specifically, we provide support and differentiated service to delay-tolerant applications with different Quality

of Service (QoS) requirements, from loss sensitive to loss tolerant. Hence, we consider the following two classes of traffic:

Class I (delay-tolerant, loss-tolerant). It may include multimedia streams that, being intended for storage or subsequent offline processing, do not need to be delivered within strict delay bounds. This class may also include scalar data or non time-critical multimedia content such as snapshots. In this case, the loss of a packet is tolerable at the current hop, but its e2e PER should still be below a specified threshold.

Class II (delay-tolerant, loss-sensitive). It may include data from critical monitoring processes that require some form of offline post processing. In this case, a packet must be retransmitted if it is not received correctly.

Our protocol employs only local information to make routing decisions, resulting in a scalable distributed solution (even though the destination information is required for routing, we can use the destination information learned from local neighbors to predict the position of the destination). It is a suboptimal solution instead of a global one since it relies on local information. The external-uncertainty regions obtained as described in Sect. IV-A are used to select the neighbor with minimum packet routing energy consumption. Here, a framework using the WHOI Micro-Modem [23] is presented. This framework can be extended and generalized in such a way as to incorporate the constraints of other underwater communication modems.

To be more specific, given the current time t_{now} [s] and a message m generated at time t_0 [s], glider i jointly optimizes the time Δt [s] to wait for the best topology configuration, a neighbor j^* , a frequency band f_{ij} , transmission power $P_{TX}^{(i,j)}(t)$ [W], packet type ξ , and number of frames⁵ $N_F(\xi)$, so that the estimated energy $E_{id}(t)$ [J] to route m to destined glider d 's region \mathcal{U}_{id} is minimized and message m reaches it within B_{max} [s], the maximum e2e delay from the source to the destination. We assume power control is possible in the range $[P_{min}, P_{max}]$ although transmission power is currently fixed for the WHOI Micro-Modem. We anticipate more advanced amplifier hardware will make this power optimization possible.

Here, $E_{id}(t)$ is estimated by the energy to transmit the packet to neighbor j in one transmission, the average number of transmissions $\hat{N}_{TX}^{(i,j)}(t)$ to send m to j , and the estimated number of hops $\hat{N}_{hop}^{(j,d)}(t)$ to reach region \mathcal{U}_{id} via j . We need to estimate the transmission power and the number of hops to destination. The external-uncertainty region is used to estimate the number of hops $\hat{N}_{hop}^{(j,d)}(t)$ to d via neighbor j and the lower bound of the transmission power as follows (Fig. 4). Let $\hat{l}_{i,p_1,p_2}(t)$ [m] be the projected distance of line segment from i to position p_1 on the line from i to position p_2 , and $l_{i,p}(t)$ be the distance from i to position p . $\hat{N}_{hop}^{(j,d)}(t)$ is estimated by the worst case of $l_{i,p}(t)/\hat{l}_{i,p_1,p_2}(t)$, i.e., (8). The lower bound for transmission power is estimated by the average transmission power so that the received power at every point in \mathcal{U}_{ij} is above the specified threshold P_{TH} . The transmission power lower bound is the integral of the product of the transmission power

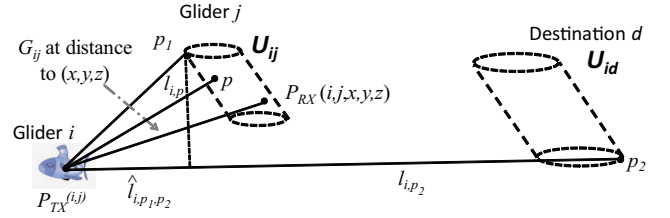


Fig. 4. Use of external-uncertainty region in the optimization framework.

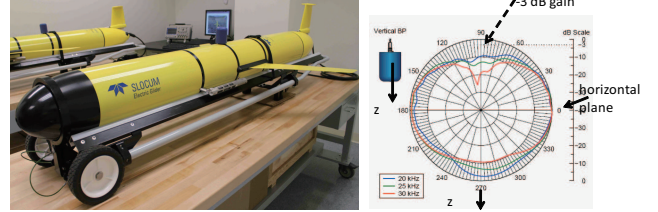


Fig. 5. Picture of our underwater glider and radiation pattern of the BT-25UF transducer.

to obtain P_{TH} at a point in \mathcal{U}_{ij} and the probability density function (pdf) of j to be at this point.

To estimate the received power, it is necessary to estimate the transducer gains at the transmitter and receiver. To estimate the transmitter's gain $G_{TX}(\theta_{ij}, \phi_{ij}, f_{ij})$, i needs to compute the radiation angles – the horizontal angle $\theta_{ij} \in [-180^\circ, 180^\circ]$ and the vertical angle $\phi_{ij} \in [-90^\circ, 90^\circ]$ with respect to j . Since the transducer is located on top of the underwater glider (Fig. 5), the relative angles of two transducers can be estimated if the pitch, yaw, and roll angles of the gliders are known. Assume the initial position of the transducer is as shown in the top left corner of Fig. 6 (i.e., upright position), then i 's normalized transducer direction vector is $\vec{n}_i = (0, 0, -1)$ with the *horizontal plane* $z = z_0^{(i)}$ (defined as the plane perpendicular to \vec{n}_i). While the glider is moving, its pitch, yaw, and roll angles are denoted by ε_i , ζ_i , and η_i , respectively. From geometry, the direction vector after rotation is $\vec{n}_i = \mathbf{Q}_x(\eta_i)\mathbf{Q}_y(\varepsilon_i)\mathbf{Q}_z(\zeta_i)\vec{n}_i^T$, while the transducer's horizontal plane is expressed as $[0, 0, 1] \cdot \mathbf{Q}_z(-\zeta_i)\mathbf{Q}_y(-\varepsilon_i)\mathbf{Q}_x(-\eta_i)[x', y', z']^T = z_0^{(i)}$, where $z_0^{(i)}$ is a constant, and $\mathbf{Q}_x(\eta_i)$, $\mathbf{Q}_y(\varepsilon_i)$ and $\mathbf{Q}_z(\zeta_i)$ are

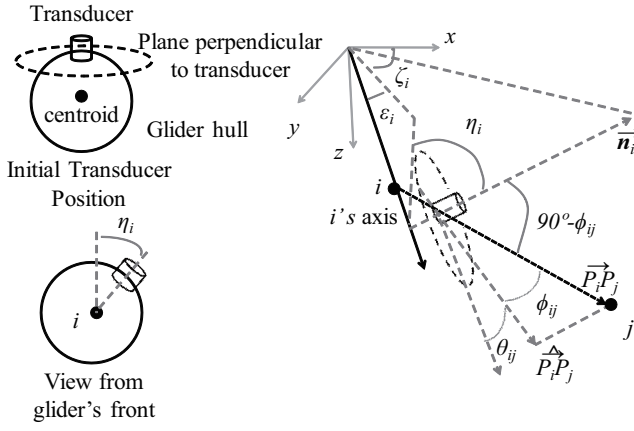
$$\begin{bmatrix} 1 & 0 & 0 \\ 0 & \cos \eta_i & -\sin \eta_i \\ 0 & \sin \eta_i & \cos \eta_i \end{bmatrix}, \begin{bmatrix} \cos \varepsilon_i & 0 & -\sin \varepsilon_i \\ 0 & 1 & 0 \\ \sin \varepsilon_i & 0 & \cos \varepsilon_i \end{bmatrix}, \begin{bmatrix} \cos \zeta_i & -\sin \zeta_i & 0 \\ \sin \zeta_i & \cos \zeta_i & 0 \\ 0 & 0 & 1 \end{bmatrix},$$

respectively.

With the position vector $\vec{P}_i\vec{P}_j$ from i to j , we can derive $\cos \phi_{ij} = \frac{\vec{P}_i\vec{P}_j \circ \vec{P}_i\vec{P}_j}{\|\vec{P}_i\vec{P}_j\| \cdot \|\vec{P}_i\vec{P}_j\|}$ and $\cos \theta_{ij} = \frac{\vec{P}_i\vec{P}_j \circ \vec{v}_i}{\|\vec{P}_i\vec{P}_j\| \cdot \|\vec{v}_i\|}$, where $\vec{P}_i\vec{P}_j$ is the projection of $\vec{P}_i\vec{P}_j$ on the transducer's horizontal plane, \circ is the inner product, and $\vec{v}_i = \|\vec{v}_i\| \cdot [\cos \varepsilon_i \cos \zeta_i, \cos \varepsilon_i \sin \zeta_i, \sin \varepsilon_i] = (a_i^*, b_i^*, c_i^*)$ is the velocity vector of glider i as estimated in Sect. IV-A. As \vec{n}_i is perpendicular to the transducer's horizontal plane, we have $\sin \phi_{ij} = \cos(90 - \phi_{ij}) = \frac{\vec{n}_i \circ \vec{P}_i\vec{P}_j}{\|\vec{P}_i\vec{P}_j\|}$ and $\vec{P}_i\vec{P}_j = \vec{P}_i\vec{P}_j - (\vec{P}_i\vec{P}_j \circ \vec{n}_i) \cdot \vec{n}_i$. The transducer's gain at receiver j , $G_{RX}(\theta_{ji}, \phi_{ji}, f_{ij})$, can be estimated in a similar way.

Let $L_m(\xi)$ be m 's length in bits depending on packet type ξ

⁵Each packet sent by WHOI Micro-Modem consists of a number of frames where the maximum number depends on ξ .

Fig. 6. Derivation of transducer angles from glider i to j .

and $B(\xi)$ be the corresponding bit rate. The energy to transmit the packet to neighbor j in one transmission can therefore be approximated by $P_{TX}^{(i,j)}(t) \cdot \frac{L_m(\xi)}{B(\xi)}$. Overall, the optimization problem can be formulated as $\mathbf{P}(\mathbf{i}, \mathbf{d}, \mathbf{t}_{\text{now}}, \Delta \mathbf{t}_p)$: **Cross-layer Optimization Problem**

Given: $P_{\min}, P_{\max}, \Xi, \Omega_\xi, G_{TX}(), G_{RX}(), \eta, B_{\max}, PER_{\max}^{e2e}$

Computed: $\varepsilon_i, \zeta_i, \varepsilon_j, \zeta_j, \mathcal{U}_{ij}, \forall j \in \mathcal{N}_i \cup \{d\}$ (i.e., $R_j^{(i)}, H_L^{(i,j)}, H_H^{(i,j)}$)

Find: $j^* \in \mathcal{N}_i, P_{TX}^{(i,j)^*}(t) \in [P_{\min}, P_{\max}],$
 $\xi^* \in \Xi, N_F^*(\xi) \in \Omega_\xi, \Delta t^*, f_{ij}^* \in [f_L, f_U]$

Minimize: $E_{id}(t) = P_{TX}^{(i,j)}(t) \cdot \frac{L_m(\xi)}{B(\xi)} \cdot \hat{N}_{TX}^{(i,j)}(t) \cdot \hat{N}_{hop}^{(j,d)}(t).$ (4)

In $\mathbf{P}(\mathbf{i}, \mathbf{d}, \mathbf{t}_{\text{now}}, \Delta \mathbf{t}_p)$, \mathcal{N}_i , Ξ , and Ω_ξ denote the set of i 's neighbors, the set of packet types, and the set of number of type ξ frames respectively. The objective function (4) estimates the energy required to send message m to the destination region \mathcal{U}_{id} . To solve this problem, we need to derive the relationship between these variables. Let $L_F(\xi)$ [bit] be the length of a frame of type ξ , L_H [bit] be the length of message m 's header, $PER(SINR_{ij}(t), \xi)$ be the PER of type ξ at the Signal to Interference-plus-Noise Ratio $SINR_{ij}(t)$, $TL(l_{ij}(t), f_{ij})$ be the transmission loss for distance $l_{ij}(t)$ and carrier frequency f_{ij} [kHz] – which is calculated using (1) – $\mathcal{A} \setminus \{i\}$ be the set of active transmitters excluding i , and $P_{TX}^{(i,j)}(t)$ be the transmission power used by i to reach j , we have the following formulas,

(class-independent relationships)

$$t = t_{\text{now}} + \Delta t; \quad (5)$$

$$t_{TTL} = B_{\max} - (t_{\text{now}} - t_0); \quad (6)$$

$$L_m(\xi) = L_F(\xi) \cdot N_F(\xi) + L_H; \quad (7)$$

$$\hat{N}_{hop}^{(j,d)}(t) = \frac{\max_{p \in \mathcal{U}_{id}} l_{i,p}(t)}{\min_{p_1 \in \mathcal{U}_{ij}, p_2 \in \mathcal{U}_{id}} \hat{l}_{i,p_1,p_2}(t)}; \quad (8)$$

$$SINR_{ij}(t) = \frac{P_{TX}^{(i,j)}(t) \cdot 10^{G_{ij}(l_{ij}(t), f_{ij})/10}}{\sum_{k \in \mathcal{A} \setminus \{i\}} P_{TX}^{(k,j)}(t) \cdot 10^{G_{ij}(l_{kj}(t), f_{ij})/10} + N_0}; \quad (9)$$

$$G_{ij}(l_{ij}, f_{ij}) = G_{TX}(\theta_{ij}, \phi_{ij}, f_{ij}) + G_{RX}(\theta_{ji}, \phi_{ji}, f_{ij}) - L_{AMP}(f_{ij}) - TL(l_{ij}, f_{ij}); \quad (10)$$

$$\theta_{ij} = \arcsin \frac{\mathbf{n}_i \circ \overrightarrow{P_i P_j}}{\|\overrightarrow{P_i P_j}\|}; \quad (11)$$

$$\phi_{ij} = \arccos \frac{\overrightarrow{P_i P_j} \circ \overrightarrow{\mathbf{v}_i}}{\|\overrightarrow{P_i P_j}\| \cdot \|\overrightarrow{\mathbf{v}_i}\|}. \quad (12)$$

Note that $N_0 = \int_{f_L}^{f_U} psd_{N_0}(f, w) df$ is the ambient noise, where $psd_{N_0}(f, w)$ is the empirical noise power spectral density (psd) for frequency band $[f_L, f_U]$ and w [m/s] is the surface wind speed as in [6]. t_{TTL} is the remaining Time-To-Live (TTL) for the packet, $L_{AMP}(f_{ij})$ [dB] is the power loss of the power amplifier at f_{ij} and PER_{\max}^{e2e} is the maximum e2e error rate for packet m . In these relationships, (5) is the time after waiting Δt ; (6) calculates the remaining TTL for message m ; (7) calculates the total message's length; (8) estimates the number of hops $\hat{N}_{hop}^{(i,j)}(t)$ to reach destination d ; (9) estimates the SINR at j while (10) estimates the total transmission gain in dB from i to j , including the transducer gain at the transmitter and receiver, loss at the power amplifier, and transmission loss; (11) and (12) estimate the transducer's radiation angles of j with respect to i . The constraints for $\mathbf{P}(\mathbf{i}, \mathbf{d}, \mathbf{t}_{\text{now}}, \Delta \mathbf{t}_p)$ are,

(class-independent constraints)

$$P_{TX}^{(i,j)}(t) \geq \int_{(x,y,z) \in \mathcal{U}_{ij}} P_{RX}(i, j, x, y, z) \cdot 10^{-G_{ij}(l_{ij}(t), f_{ij})/10} \quad (13)$$

$$\cdot g_R(x, y) \cdot g_H(z) dx dy dz; \quad (14)$$

$$P_{RX}(i, j, x, y, z) \geq P_{TH}; \quad (14)$$

$$0 \leq \Delta t \leq \frac{t_{TTL}}{\hat{N}_{TX}^{(i,j)}(t) \cdot \hat{N}_{hop}^{(j,d)}(t)}. \quad (15)$$

In these constraints, $P_{RX}(i, j, x, y, z)$ is the received signal power at the generic 3D location (x, y, z) when i transmits to j . Last, $g_R(x, y)$ and $g_H(z)$ are the pdfs of the glider's position on the horizontal plane (i.e., χ -distribution with degree of $2N - 2$) and on the vertical direction (i.e., Student's t -distribution with $N - 1$ degrees of freedom), respectively [8], P_{TH} is the received power threshold so that the packet can be received with a certain predefined probability. (IV-B) estimates the lower bound of the transmission power to cover the external-uncertainty region so that the received power is above a pre-specified threshold, as accounted for in (14); (15) estimates the bounds of Δt , which must be less than the maximum tolerable delay at the current hop. To support the two classes of delay-tolerant traffic, we have the following additional constraints,

(additional class-dependent constraints)

$$\text{Class I} = \begin{cases} \hat{N}_{TX}^{(i,j)}(t) = 1 \\ 1 - [1 - PER(SINR_{ij}(t), \xi)]^{\hat{N}_{hop}^{(j,d)}(t)} \leq PER_{\max}^{e2e} \end{cases}; \quad (16)$$

$$\text{Class II} = \left\{ \hat{N}_{TX}^{(i,j)}(t) = [1 - PER(SINR_{ij}(t), \xi)]^{-1} \right\}. \quad (17)$$

The first constraint for Class I traffic forces packet m to be transmitted only once, while the second constraint guarantees the e2e PER of m should be less than a specified threshold PER_{\max}^{e2e} . The constraint for Class II traffic guarantees message m will be transmitted for the average number of times for successful reception at j . By solving this local optimization problem every time the inputs change significantly (and not every time a packet needs to be sent), i is able to select the optimal next hop j^* so that message m is routed (using minimum network energy) to the external-uncertainty region \mathcal{U}_{id} where destination d should be. Obviously different objective functions (e2e delay, delivery ratio, throughput) could be used depending on the traffic class and mission QoS requirements. Note that in fact our solution can be extended to serve two other classes of traffic - 1) delay-sensitive, loss-tolerant traffic,

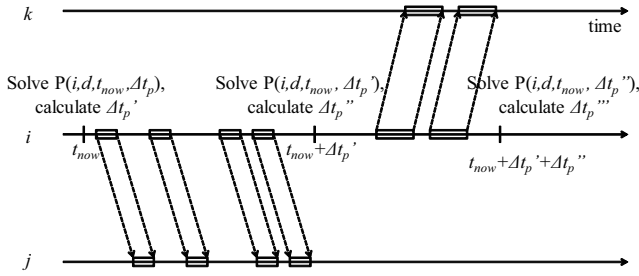


Fig. 7. Solving $P(i, d, t_{now}, \Delta t_p)$ every Δt_p at i .

and 2) delay-sensitive, loss-sensitive traffic - by setting Δt to 0 (the delay discussed here can be hours or days as these AUVs move slow in the vast ocean).

To reduce the complexity, we can convert $P(i, d, t_{now}, \Delta t_p)$ into a discrete optimization problem by considering finite sets of $P_{TX}^{(i,j)}$ and Δt , which can be taken to be a number of equally spaced values within their respective ranges. The problem then can be solved by comparing the e2e energy consumption estimates of different combination of these discrete values. Assuming that transmission power and time are discretized into N_P and N_{time} values, respectively, for the case of WHOI modem (3 frequencies and 14 combinations of packet type and number of frames [8]), the processor in node i needs to calculate the objective value $42N_P \cdot N_{time} \cdot |\mathcal{N}_i|$ times in each round. The embedded Gumstix motherboard (400 MHz processor and 64 MB RAM) attached to the Micro-Modem is adequate to solve such a problem. To further reduce the computation, instead of running the solution for every packet, it will be rerun only at $t_{now} + \Delta t_p$ for the same class of traffic flow that is sent from i to the same destination d . Here, Δt_p is taken as the minimum of the Δt values of the packets belonging to the same class of traffic and the same destination, estimated from the previous run. Figure 7 depicts an example of how $P(i, d, t_{now}, \Delta t_p)$ is solved at i . At time t_{now} , the problem is solved with j found to be the next hop to d . The minimum of the Δt values of these packets belonging to the same class of traffic and the same destination observed before t_{now} is $\Delta t_p'$. Packets for d will then be forwarded to j with the calculated transmission power at the selected frequency band until $t_{now} + \Delta t_p'$. Then, the problem is solved again and k is found to be the next hop. The minimum Δt observed so far is $\Delta t_p''$ and, hence, the problem will be solved at $t_{now} + \Delta t_p' + \Delta t_p''$.

Once the optimal frequency band is selected, i needs to notify j to switch to the selected band. A simple protocol can be used as follows. All AUVs use the same frequency band as the Common Control Channel (CCC) to tell the receiver which band is selected. A short packet or preamble with the selected band number is first sent by the transmitter using the CCC, followed by the data packet using selected frequency band after the time for the transmitter and receiver to finish frequency band switching. The receiver will first listen on the CCC, switch to the selected band embedded in the short control packet or preamble, receive the data packet, and then send back a short ACK packet to acknowledge the reception. Finally, both sides switch back to the CCC if the transmission

succeeds or the transmission times out. The time out period is set long enough to make sure the ACK packet replied within the transmission range will be received with specified probability. Retransmission (with limited number) will be triggered if the transmission times out. More sophisticated frequency-band switching protocols, which are out of the scope of this paper, can be designed to improve network performance. We rely on the Medium Access Control (MAC) scheme with the WHOI modem to send the data. Since the speed of acoustic wave underwater is very slow when compared with radio waves, the propagation delay has to be considered in order to avoid packet collisions. However, it is difficult to estimate the propagation delay since the positions are uncertain. It may not improve the performance much as the actual propagation delay may be different from the estimation. Moreover, the inter-vehicle traffic underwater is generally low. So the problem of packet collisions is not severe and hence we can just use the onboard MAC scheme.

C. Discussion

Studying the impact of an unreliable wireless channel on networked systems (such as underwater acoustic channel) has been a hot research topic over the years. Many theoretical works have been proposed to study the performance bounds of networked control systems or wireless sensor networks when the wireless channel is unreliable. Some works [32], [33] focused on the analysis or design of source encoding, channel encoding, decoding, and controller for optimality of system performance. In [32], a new concept called anytime capacity is defined to study the problem of communicating the delay-sensitive data of an unstable discrete-time Markov random process through a noisy channel. Source coding, channel coding and delay sensitivity are studied and a new source/channel separation theorem is given for delay-sensitive data, which is shown to be useful in control systems. There are also works that focus on the analysis and design of optimal estimation and control in the networked systems. For example, the work in [34] seeks to synthesize the optimal information flow and control under given communication network constraints. A joint design of the information flow and the control to achieve optimal estimation and control is proposed, and it is shown to benefit system stability and performance.

In this work, we focus on the optimization of inter-vehicle communications among networked mobile AUVs instead of optimal control performance. Moreover, we consider the constraints of existing communication modems, which have limited modulation and channel coding options. Our goal here is to have a solution that will be used in practice to optimize the inter-vehicle communications. A more thorough theoretical analysis of the proposed optimization framework, such as the study of capacity bounds for inter-vehicle communications and the impact on AUV control performance, is left as a future work.

V. PERFORMANCE EVALUATION

The communication solution is implemented and tested on our underwater communication emulator [8] as shown in Fig. 8. This underwater acoustic network emulator is

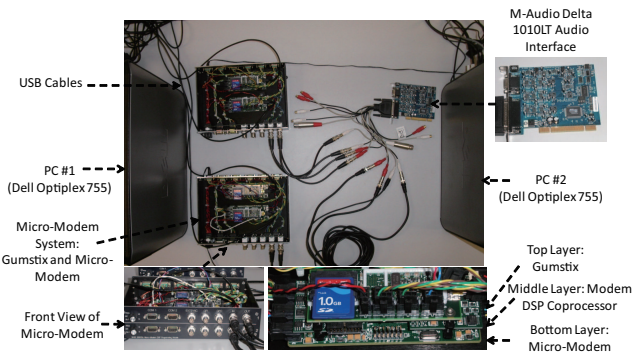


Fig. 8. Underwater communication emulator using WHOI Micro-Modems.

composed of four WHOI Micro-Modems [23] and a real-time audio processing card to emulate underwater channel propagation. The multi-input multi-output audio interface can process real-time signals to adjust the acoustic signal gains, to introduce propagation delay, to mix the interfering signals, and to add ambient/man-made noise and interference. Due to the limited number of Micro-Modems and audio processing channels, we can only mix signals from up to three transmitters at the receiver modem (one as the receiver and the other three as the transmitters). Therefore, we calculate, select for transmission, and mix with ambient noise, only the three most powerful signals the receiver will encounter. We leave the simulation of more than three simultaneously transmitted signals as a problem for further research.

We are interested in evaluating the performance of the proposed solution in terms of e2e energy consumption, e2e reliability (i.e., e2e delivery ratio), average bit rate of a link, and overhead, under an environment that is described by the Bellhop model (and the Munk acoustic speed profile as input).

Assume that a glider's drifting (i.e., the relative displacement from the glider's trajectory) is a 3D random process $\{X(t), t \geq 0\}$ as the following [35]: 1) In the beginning of the deployment, the drifting is 0, i.e., $X(0) = (0, 0, 0)$; 2) The drifting has independent increments, in that for all $0 \leq t_1 < t_2 < \dots < t_n$, $X(t_n) - X(t_{n-1})$, $X(t_{n-1}) - X(t_{n-2})$, \dots , $X(t_2) - X(t_1)$, $X(t_1)$ are independent; 3) The drifting has stationary increments, in that the distribution of $X(t+s) - X(t)$ does not depend on t and is normally distributed with zero mean and covariance matrix $s\sigma^2 I_3$, where I_3 is the 3×3 identity matrix, and σ is a scaling factor that decides the magnitude of drifting. Note that this drifting model is ideal since the drifting in any of the x, y, z directions is Gaussian. The consideration of realistic drifting pattern is left as future work. Emulation parameters are listed in Table I. The radiation pattern of the BT-25UF transducer (Fig. 5) is used in the emulations. Every 10 seconds, a packet is generated in each node. A glider is randomly selected as the collector and half of the other gliders are randomly selected to forward their packets towards it. For statistical relevance, emulations are run for 50 rounds and the average is plotted with 95% confidence interval. Note that it actually is a scenario for deep water. We will also evaluate the performance in shallow water, where acoustic waves propagate differently.

We are interested in evaluating the performance of our

TABLE I
EMULATION SCENARIO PARAMETERS

Parameter	Value
Deployment 3D region	2500(L) \times 2500(W) \times 1000(H) m ³
Confidence Parameter α	0.05
$[P_{min}, P_{max}]$	[1, 10] W
Packet Types Ξ	{0, 2, 3, 5}
Glider Horizontal Speed	0.3 m/s
Gliding Depth Range	[0, 100] m
Carrier Frequencies	10, 15, 25 kHz
B_{max}	10 hr

solution for the two classes of traffic in Sect. IV-B, using either the BT-25UF transducer or an ideal omni-directional transducer (with gain equal to 0 dBi). We also want to compare the performance of our solution, which delays the transmission for optimal topology configuration, with the solution without delaying the transmission. For convenience, we denote, respectively, QUO VADIS for Class I traffic using the BT-25UF transducer by 'QUO VADIS I', for Class I traffic using the ideal omni-directional transducer by 'QUO VADIS I - OMNI', for Class II traffic using the BT-25UF transducer by 'QUO VADIS II', for Class II traffic using the ideal omni-directional transducer by 'QUO VADIS II - OMNI', and the solution with no delaying of the transmission (i.e., $\Delta t = 0$ for $\mathbf{P}(i, d, t_{now}, \Delta t_p)$) by 'QUO VADIS - ND'. We will also compare the performance of our solution with geographical routing solutions – MFR, GRS, CRM, and PTKF – and DTN solutions – RAPID, Spray and Wait, and MaxProp – as review in Sect. II. To make the comparison fair, we use two variant protocols for each of these solutions by adding the constraints of the two classes of traffic to these solution. For example, we denote the MFR solution with Class I constraints in (16) by 'MFR I', and the solution with Class II constraints in (17) by 'MFR II'.

The following networking metrics are compared:

- **e2e energy consumption:** the average energy consumed to route one bit of data to the destination;
- **e2e delivery ratio:** the number of data packets received correctly over the number of data packets sent;
- **link bit rate:** the average bit rate between a transmission pair;
- **overhead:** the number of bytes used for position and control to facilitate the transmission of payload data.

Emulations are done for different settings and the results are plotted with 95% confidence interval and discussed in the following subsections.

A. Comparison With Geographic Routing Protocols

We compare the performance of our solution with geographic routing protocols in Figs. 9 and 10. As shown in these two figures, we can see that QUO VADIS has better performance than QUO VADIS - OMNI and QUO VADIS - ND for the same class of traffic in terms of these three metrics. By delaying packet transmissions to wait for the optimal network topology, the e2e energy consumption is reduced while the e2e delivery ratio and link bit rate increase (e.g., with 5 gliders, the energy consumption for QUO VADIS I is around 30% of that for QUO VADIS-ND). By exploiting

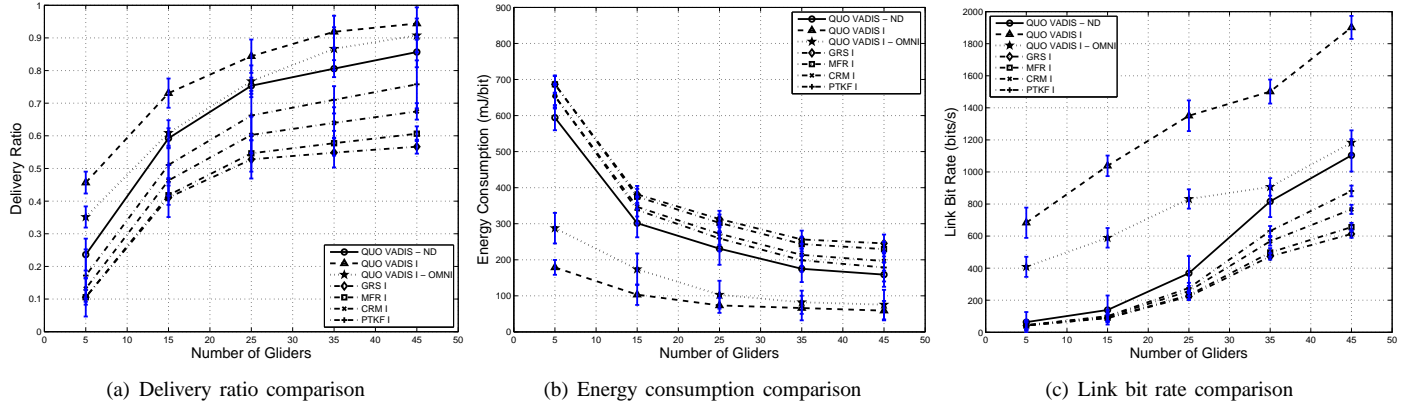


Fig. 9. Performance comparison for Class I traffic with *geographic routing* protocols.

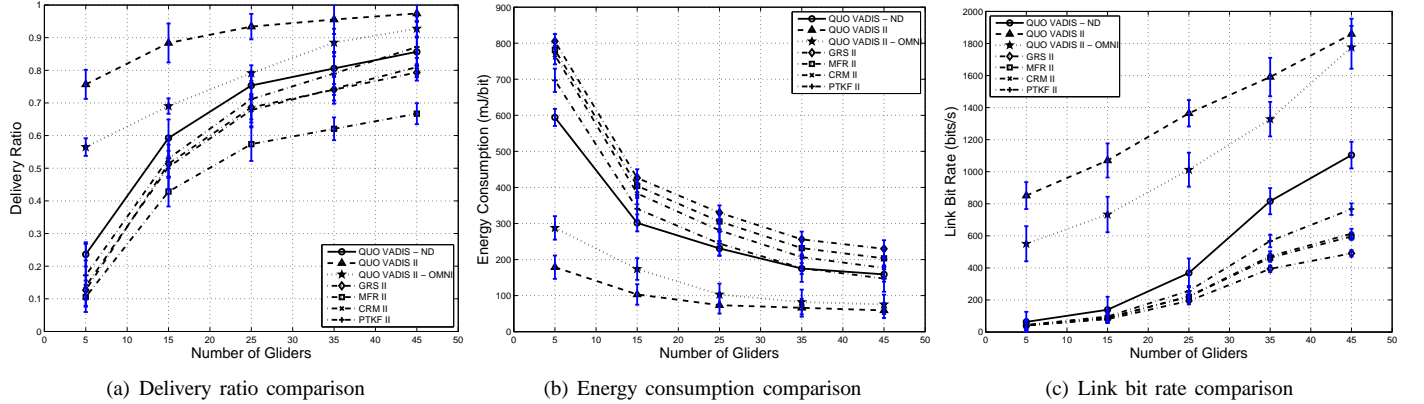


Fig. 10. Performance comparison for Class II traffic with *geographic routing* protocols.

the frequency-dependent radiation pattern of the transducer, received signal power may obtained a gain of up to 20 dB, which we observed in the simulations. Hence QUO VADIS using the BT-25UF transducer has better performance than that using the omni-directional transducer. Due to the QoS requirements, retransmissions are needed to recover link errors, resulting in higher e2e delivery ratio for Class II traffic than for Class I traffic. On the other hand, this leads to more energy consumption.

Different versions of our QUO VADIS solutions also perform better than geographic routing protocols GRS, MFR, CRM and PKTF. This is because that uncertainty in location leads to errors in route selection, packet transmissions and transmission power estimates. Also these geographic routing protocols do not consider the propagation delay underwater, which results in degraded communication performance. Interesting enough, we can see that among these geographic routing protocols, PKTF offers the best performance. This is because it jointly considers the transmission power and routing to minimize the e2e energy consumption. Therefore it performs better than the other geographic routing protocol, which only consider the distance or angle metrics for routing (not closely related to network performance). GRS gives the worst performance since it generally needs to forward the packet to the node that is far from the transmitter, which introduces bad link performance. Similarly, CRM performs better than MFR as the CRM has less probability to forward

packets to node that is far away than MFR does.

B. Comparison with DTN Solutions

We further compare QUO VADIS with the DTN solutions – RAPID, MaxProp and Spray and Wait. As shown in Figs. 11 and 12, QUO VADIS gives improved performance over RAPID, MaxProp and Spray and Wait. This is mainly due to that these DTN solutions transfer packets once the neighbors are in the transmission range. Such schemes may be good for scenarios where the connectivity is intermittent. However, the performance may not be optimal since this may not be the time to achieve the best link performance. In contrast, QUO VADIS predicts and waits for the best network configuration, where nodes move closer for the best communications. So the e2e delivery ratio and link bit rate of QUO VADIS is the highest while its energy consumption is minimal. Note that among these compared DTN solutions, RAPID performs the best. This is because RAPID prioritizes old packets so they won't be dropped. MaxProp gives priority to new packets; older, undelivered packets will be dropped in the middle. Spray and Wait works in a similar way, which does not give priority to older packets. On the other hand, Spray and Wait is slightly better than MaxProp. This is because in our scenario, the network connectivity is not disrupt. The way MaxProp routes based on the e2e delivery ratio estimation will be very different from that Spray and Wait does, i.e., just transmits the packet to a neighbor then lets the neighbor continue to forward

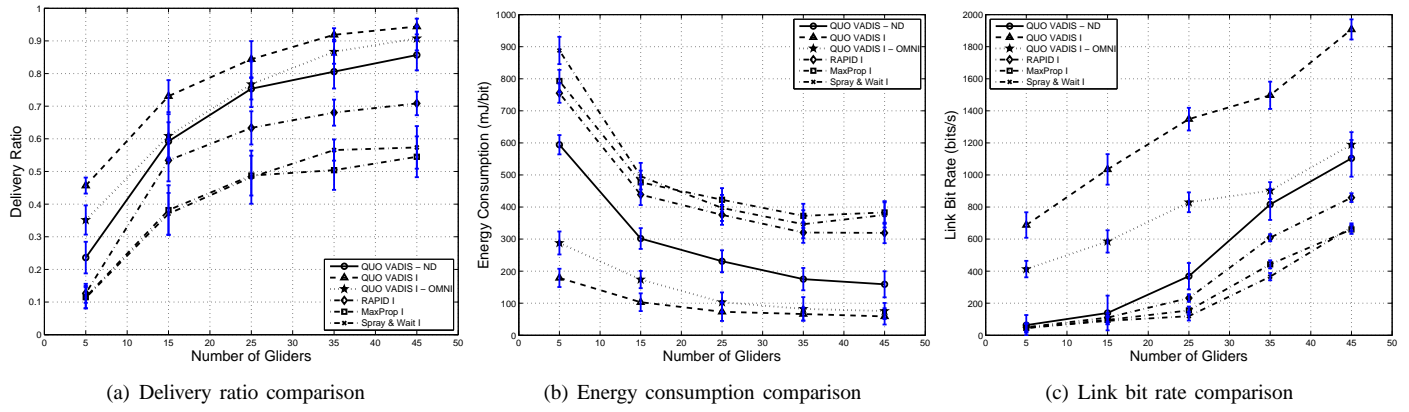


Fig. 11. Performance comparison for Class I traffic with DTN protocols.

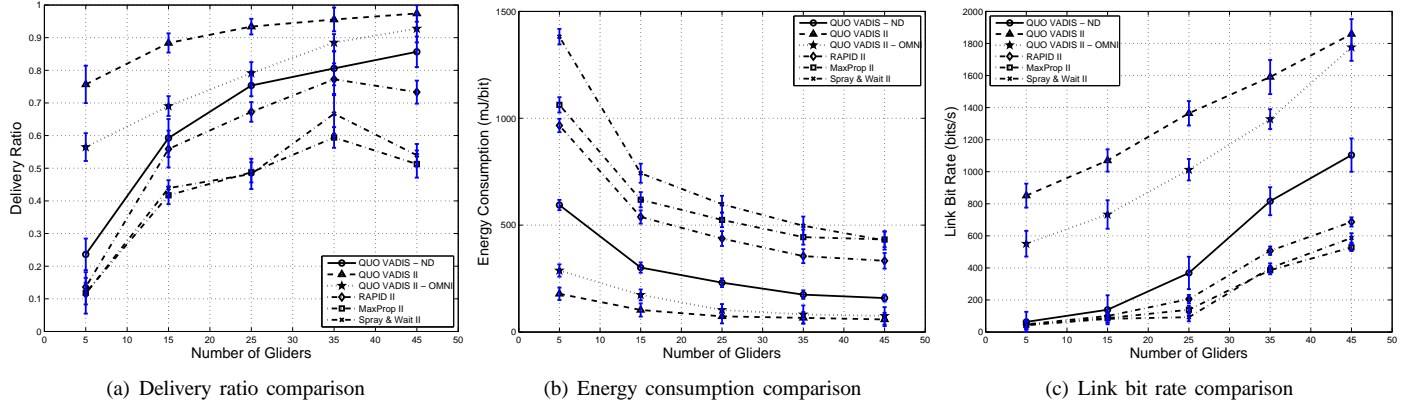


Fig. 12. Performance comparison for Class II traffic with DTN protocols.

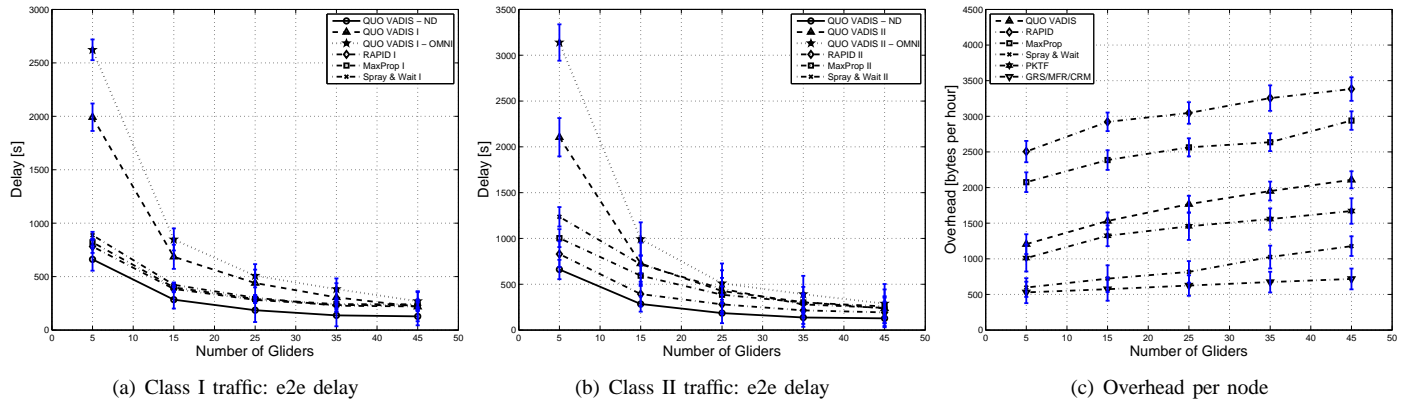


Fig. 13. Comparison of e2e delay and overhead.

it. Moreover, MaxProp still needs to pay for the overhead to obtain the global e2e delivery ratio information.

C. End-to-end Delay Comparison

To see QUO VADIS can meet the delay requirement of the delay-tolerant traffic, we also calculate and plot the e2e delays of these solutions. As shown in Figs. 13(a) and 13(b), QUO VADIS - ND gives the least e2e delay. Compared to QUO VADIS and QUO VADIS - OMNI, QUO VADIS - ND does not wait for the vehicles to move to the optimal configuration yet more retransmissions are necessary. As the vehicle speed is much slower than the acoustic speed, QUO VADIS - ND

still needs much less time than QUO VADIS and QUO VADIS - OMNI even though more retransmissions are needed (thus resulting in more communication delay). Similarly, the huge difference between vehicle speed and acoustic speed leads to the result that QUO VADIS and QUO VADIS - OMNI need more time than the DTN protocols (RAPID, MaxProp, and Spray and Wait), especially when the number of vehicles is small (where average inter-vehicle distance is large). On the other hand, by taking the position uncertainty into account, communications using QUO VADIS - ND is more reliable than those using RAPID, MaxProp or Spray and Wait so less delay is incurred. QUO VADIS has less delay than QUO

VADIS - OMNI due to the improvement in communications by exploiting the directional transducer gain. Also Class II traffic generally has more e2e delay than Class I due to the need for retransmissions. Last, note that as the number of gliders increases, the delays of QUO VADIS and QUO VADIS - OMNI drop quickly. This is because average inter-vehicle distance becomes smaller and the number of close neighbors increases, which reduces the need for a glider to wait a long time until a neighbor moves close.

D. Overhead Comparison

We plot and compare the overheads (per node) of these protocols in Fig. 13(c). Note that as QUO VADIS, QUO VADIS - ND, and QUO VADIS - OMNI work almost the same way, i.e., the uncertainty region information is broadcast periodically (here the period is taken to be 60 s), their overheads are the same and thus we use QUO VADIS in the figure to represent these variant versions. Similarly, nodes running the geographic routing protocols GRS, MFR and CRM only need to periodically broadcast the position information so their overhead is basically the same. Hence we use GRS/MFR/CRM to represent them.

Surprisingly, even though QUO VADIS achieves the best network performance, its overhead is not the biggest. The protocols with the larger overhead are RAPID and MaxProp. In order to work, RAPID needs the following control information: average size of past transfer opportunities, expected meeting times with nodes, list of packets delivered since last exchange, the updated delivery delay estimate based on current buffer state, and information about other packets if modified since last exchange with the peer, which takes a large number of bytes. MaxProp needs to exchange a list of the probabilities of meeting every other node on each contact, which is basically global information. It also has the neighbor discovery overhead. Compared to RAPID and MaxProp, QUO VADIS only needs to exchange the external uncertainty information of itself and the destination node, which is obviously less. On the other hand, PKTF needs a probe message that has five data fields. Only the nodes in the selected path are required to respond with a probe – whether it is sent for the forwarding or reverse direction. The Spray and Wait protocol reduces transmission overhead by spreading only a few number of data packets to the neighbors. The source node then stops forwarding and lets each node carrying a copy perform direct transmission. In our emulation, we select the number to be one to make the comparison fair and hence the overhead is small. Lastly, for the other geographic routing protocols GRS, MFR and CRM, the nodes just need to know the geographic locations of the neighbors and the destination. Therefore the overhead required is the least. Note that here it is not necessary to differentiate the two classes of traffic since the overhead difference is small.

E. Performance in Shallow Water

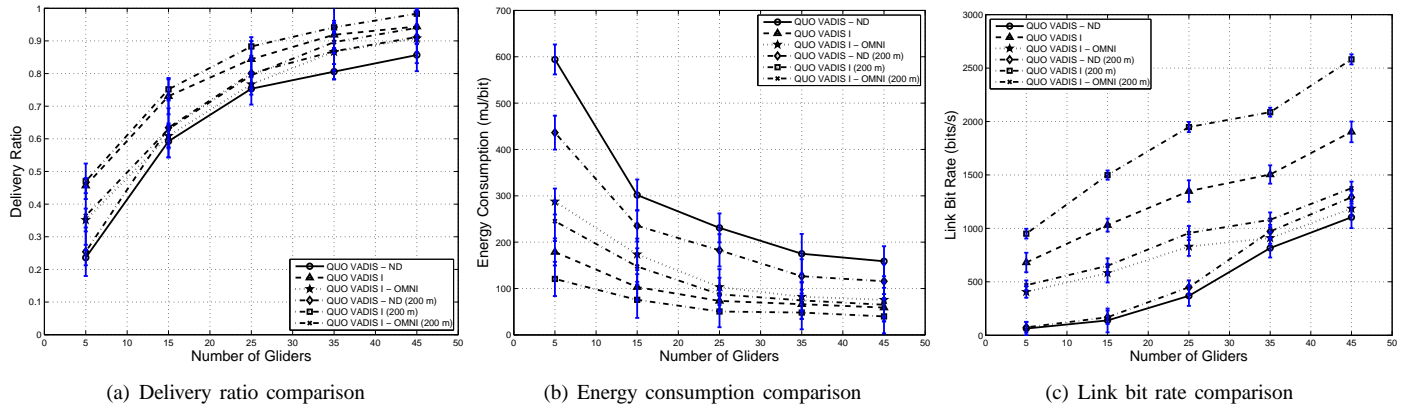
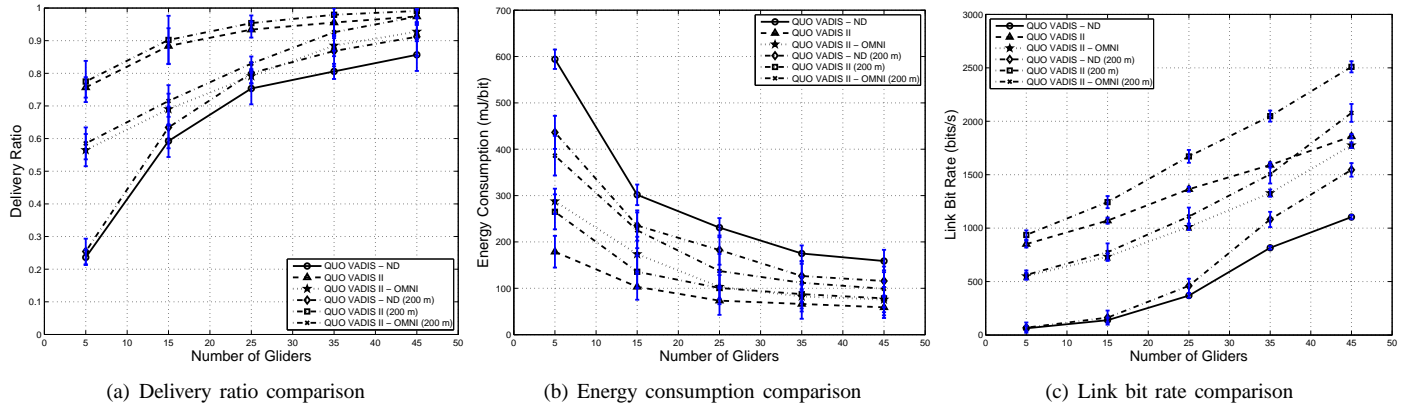
So far the results are obtained using the setting in Table I, which is for the deep water. We change the network scenario to the shallow water scenario by setting the depth of the 3D region to 200 m. In this shallow water scenario, the path

loss estimated by the Urlick's model is very different from that estimated by the Bellhop model. We had anticipated the performance will degrade because of this mismatch. Surprising enough, as shown in Fig. 14 and 15, we find the performance (in terms of e2e delivery ratio, energy consumption, and link bit rate) in the shallow water is actually better. A more careful analysis reveals the reason – the existence of the *surface duct* in the shallow water. Surface duct is basically a zone below the sea surface where sound rays are refracted toward the surface and then reflected. The rays alternately are refracted and reflected along the duct out to relatively long distances from the sound source. Hence the acoustic waves are relatively concentrated in the surface duct, leading to less path loss. This consequently leads to improved network performance.

F. Performance using Different Uncertainty Update Intervals

Emulations so far have been fixing broadcast interval of uncertainty region to 60 s. Our last interest is to evaluate the performance of the QUO VADIS variants when different broadcast intervals are used. Therefore we re-run the emulations for two more cases: i) half of interval (i.e., 30 s); and ii) double of interval (i.e., 120 s). From Fig. 16 and 17, we can see that the performance of the QUO VADIS variants becomes worse when the update interval is doubled. This is because when the interval is doubled, the position uncertainty information becomes less accurate. This leads to larger error in selection of neighbor for packet forwarding and estimation of transmission power. On the other hand, halving the interval leads to improvement of performance due to the uncertainty information is updated in a more timely manner (so routing error becomes smaller and transmission power is better estimated). However, this obviously leads to the overhead increase. Therefore the tradeoff between overhead and metrics such as delivery ratio, energy consumption and link bit rate should be carefully considered for different applications. Here we use “QUO VADIS - Half”, “QUO VADIS”, and “QUO VADIS - Twice” to denote the cases with update interval of 30 s, 60 s and 120 s, respectively.

To find out the optimal update interval, depending on the need, we can define an objective function that jointly considers the tradeoff between performance metrics such as the e2e energy consumption and overhead. For example, to find the optimal update interval for e2e energy consumption, we can define an objective function as $f_{\text{obj}}(E_{e2e}, R_{e2e}, O, |\mathcal{N}|) = E_{e2e} \cdot R_{e2e} / (O \cdot |\mathcal{N}|)$, which characterizes the e2e energy consumption per overhead bit per node. In this objective function, E_{e2e} [J/bit] is the e2e energy consumption as previously defined, R_{e2e} [bit/s] is the e2e bit rate, O [bit/s] is the overhead as previously defined, and $|\mathcal{N}|$ is the number of gliders. Emulations are run for different update intervals for class I traffic and the results are plotted in Fig. 18. From this figure, we can see that as update interval increases, f_{obj} decreases first and then increases. This is because that when the update interval is increasing from a small value, the redundant overhead generated is decreased, leading to decrease in the energy spent in overhead and the decrease in e2e bit rate (due to the decrease in estimation accuracy). As the update interval increases more, the increase in uncertainty estimation

Fig. 14. *Shallow water*: performance comparison for Class I traffic.Fig. 15. *Shallow water*: performance comparison for Class II traffic.

leads to more data retransmission (and therefore more energy consumption). Hence the e2e energy consumption increases again. From Fig. 18(a), we can find the optimal update interval for different versions of our solution. We can see that QUO VADIS I has the largest optimal update interval and QUO VADIS I - ND has the smallest optimal update interval, since the increase of position estimation error (due to increase in update interval) can be offset by good communication performance. The optimal update intervals for different number of gliders are also shown in Fig. 18(b). We can see that as $|\mathcal{N}|$ increase the optimal update interval also increase for QUO VADIS I. This is because the increase in estimation error can be offset by the increase of possible neighbors for packet forwarding. Similar results can be observed for class II traffic. Due to space limitation, we skip plotting them here.

VI. CONCLUSION

We proposed QUO VADIS, a **QoS-aware underwater optimization framework for inter-vehicle communication using acoustic directional transducers**. Based on the trajectory and position uncertainties of the AUVs, an AUV predicts a favorable network topology with relatively short links in the future and postpones transmission in favor of a lower transmission energy and a higher data rate. Communication energy consumption is further reduced by exploiting the frequency-dependent radiation pattern of underwater acoustic transducers. The proposed solution is implemented and tested in our

underwater communication emulator, showing improvement over some well-known geographic routing protocols and DTN protocols in terms of e2e energy consumption, reliability, and link bit rate.

REFERENCES

- [1] B. Chen and D. Pompili, "QUO VADIS: QoS-aware underwater optimization framework for inter-vehicle communication using acoustic directional transducers," in *Proc. 2011 IEEE Communications Society Conference on Sensor, Mesh, and Ad Hoc Communications and Networks*.
- [2] I. F. Akyildiz, D. Pompili, and T. Melodia, "Underwater acoustic sensor networks: research challenges," *Ad Hoc Networks (Elsevier)*, vol. 3, no. 3, pp. 257–279, May 2005.
- [3] X. Xiang, Z. Zhou, and X. Wang, "Self-adaptive on demand geographic routing protocols for mobile ad hoc networks," in *Proc. 2007 IEEE International Conference on Computer Communications*.
- [4] J. M. Montana, M. Stojanovic, and M. Zorzi, "Focused beam routing protocol for underwater acoustic networks," in *Proc. 2008 ACM International Workshop on Underwater Networks*.
- [5] D. Pompili and I. F. Akyildiz, "A cross-layer communication solution for multimedia applications in underwater acoustic sensor networks," in *Proc. 2008 IEEE International Conference on Mobile Ad-hoc and Sensor Systems*.
- [6] M. Stojanovic, "On the relationship between capacity and distance in an underwater acoustic communication channel," in *Proc. 2006 ACM International Workshop on UnderWater Networks*.
- [7] K. Fall, "A Delay-Tolerant Network Architecture for Challenged Internets," in *Proc. 2003 ACM Special Interest Group on Data Communication*.
- [8] B. Chen, P. Hickey, and D. Pompili, "Trajectory-aware communication solution for underwater gliders using WHOI micro-modems," in *Proc. 2010 IEEE Communications Society Conference on Sensor, Mesh, and Ad Hoc Communications and Networks*.

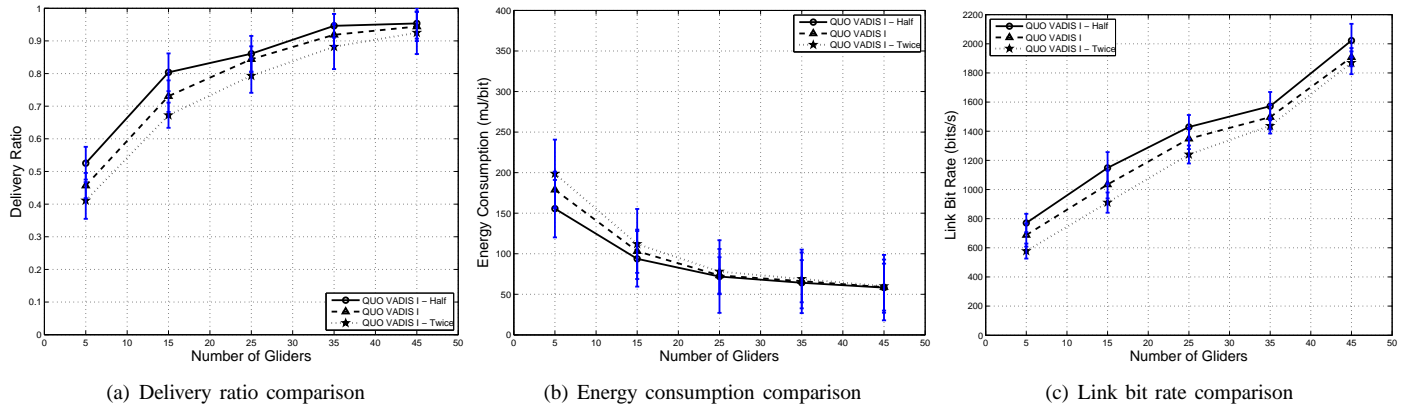
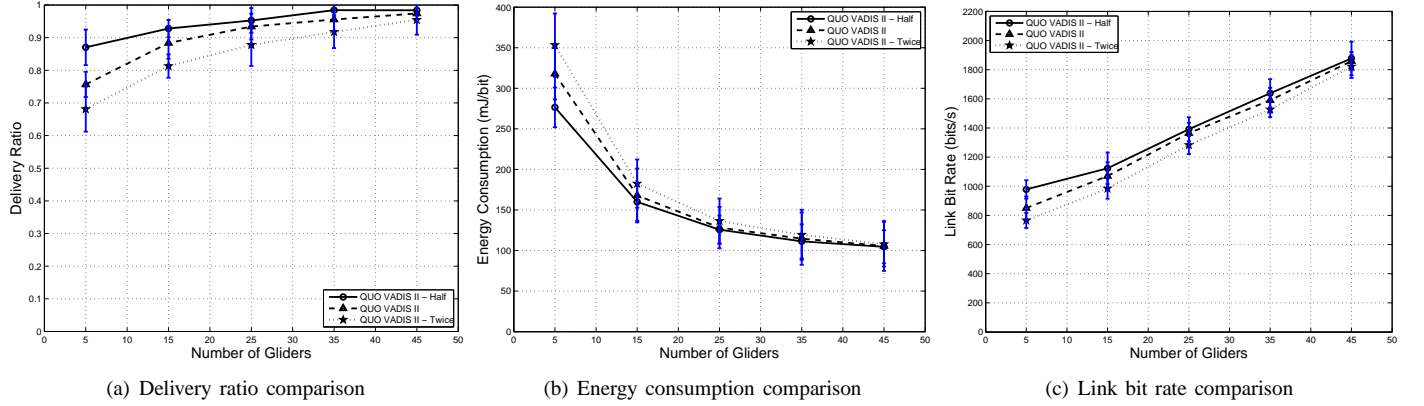
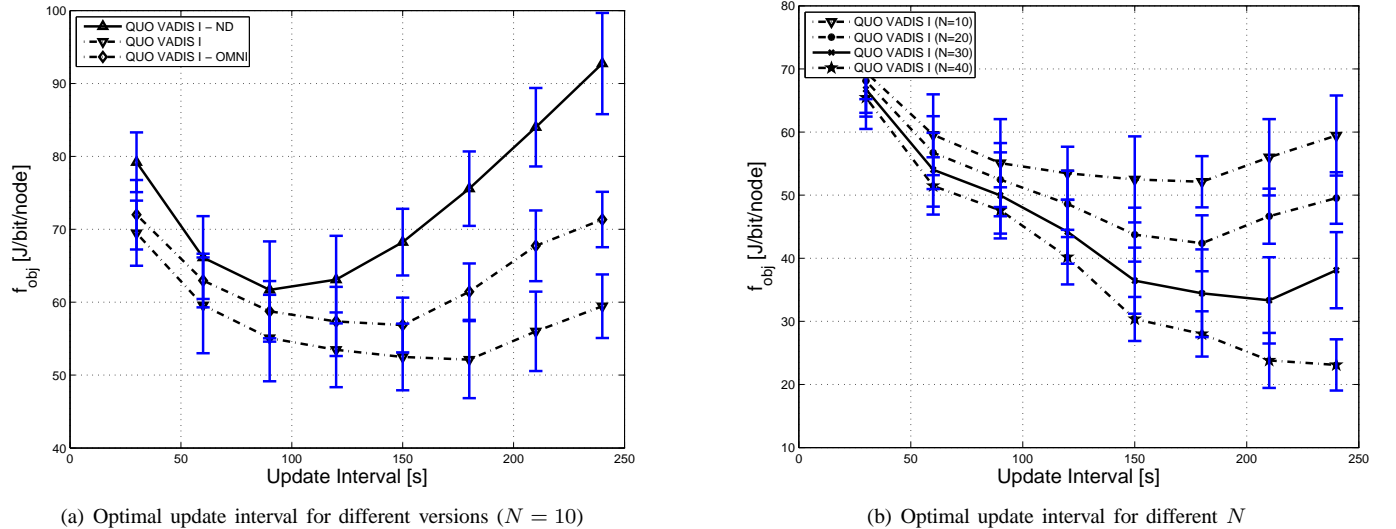
Fig. 16. *Uncertainty update interval*: performance comparison for Class I traffic.Fig. 17. *Uncertainty update interval*: performance comparison for Class II traffic.

Fig. 18. Optimal update interval.

- [9] H. Takagi and L. Kleinrock, "Optimal transmission ranges for randomly distributed packet radio terminals," *IEEE Trans. Commun.*, vol. COM-32, no. 3, pp. 246–257, Mar. 1984.
- [10] G. G. Finn, "Routing and addressing problems in large metropolitan scale Internetworks," ISI, Storrs, CT, Tech. Rep., 1987.
- [11] E. Kranakis, H. Singh, and J. Urrutia, "Compass routing on geometric networks," in *Proc. 1999 Canadian Conference on Computational Geometry*.
- [12] T. Melodia, D. Pompili, and I. F. Akyildiz, "On the interdependence of distributed topology control and geographical routing in ad hoc and

- sensor networks," *IEEE J. Sel. Areas Commun.*, vol. 23, no. 3, pp. 520–532, Mar. 2005.
- [13] S. Burleigh, A. Hooke, L. Torgerson, K. Fall, V. Cerf, B. Durst, K. Scott, and H. Weiss, "Delay-tolerant networking: an approach to interplanetary internet," *IEEE Commun. Mag.*, vol. 41, no. 6, pp. 128–136, June 2003.
- [14] A. Balasubramanian, B. Levine, and A. Venkataramani, "DTN routing as a resource allocation problem," in *Proc. 2007 ACM Conference on Applications, Technologies, Architectures, and Protocols for Computer Communications*.
- [15] T. Spyropoulos, K. Psounis, and C. S. Raghavendra, "Spray and wait: an

- efficient routing scheme for intermittently connected mobile networks,” in *Proc. 2005 ACM SIGCOMM Workshop on Delay-Tolerant Networking*.
- [16] J. Burgess, B. Gallagher, D. Jensen, and B. N. Levine, “MaxProp: routing for vehicle-based disruption-tolerant networks,” in *Proc. 2006 Conference on Computer Communications*.
- [17] C. Y. Chan and M. Motani, “An integrated energy efficient data retrieval protocol for underwater delay tolerant networks,” in *Proc. 2007 IEEE International Conference on Engineering in the Ocean Environment (OCEANS)*.
- [18] Z. Guo, G. Colombi, B. Wang, J.-H. Cui, and D. Maggiorini, “Adaptive routing in underwater delay/disruption tolerant sensor networks,” in *Proc. 2008 IEEE/IFIP Conference on Wireless on Demand Network Systems and Services*.
- [19] Z. Guo, B. Wang, and J.-H. Cui, “Prediction assisted single-copy routing in underwater delay tolerant networks,” in *Proc. 2010 IEEE Global Communications Conference*.
- [20] E. Magistretti, J. Kong, U. Lee, M. Gerla, P. Bellavista, and A. Corradi, “A mobile delay-tolerant approach to long-term energy-efficient underwater sensor networking,” in *Proc. 2007 IEEE Wireless Communications and Networking Conference*.
- [21] H. Luo, Z. Guo, W. Dong, F. Hong, and Y. Zhao, “LDB: localization with directional beacons for sparse 3D underwater acoustic sensor networks,” *J. Networks*, vol. 5, no. 1, pp. 28–38, Jan. 2010.
- [22] P. Xie, J. H. Cui, and L. Lao, “VBF: vector-based forwarding protocol for underwater sensor networks,” in *Proc. 2005 IFIP Networking*.
- [23] L. Freitag, M. Grund, S. Singh, J. Partan, P. Koski, and K. Ball, “The WHOI micro-modem: an acoustic communications and navigation system for multiple platforms,” in *Proc. 2005 IEEE International Conference on Engineering in the Ocean Environment (OCEANS)*.
- [24] M. Porter, “BELLHOP Gaussian Beam/Finite Element Beam Code,” <http://oalib.hlsresearch.com/Rays/index.html>.
- [25] F. B. Jensen, W. A. Kuperman, M. B. Porter, and H. Schmidt, *Computational Ocean Acoustics*, 2nd ed. American Institute of Physics, 1997.
- [26] W. S. Burdick, “Underwater acoustic system analysis,” in *Prentice-Hall Signal Processing Series*, A. V. Oppenheim, Ed. Prentice-Hall, 1984, ch. 2, p. 49.
- [27] E. Olson, J. J. Leonard, and S. Teller, “Robust range-only beacon localization,” *IEEE J. Ocean. Eng.*, vol. 31, no. 4, pp. 949–958, Oct. 2006.
- [28] M. F. Fallon, G. Papadopoulos, J. J. Leonard, and N. M. Patrikalakis, “Cooperative AUV navigation using a single maneuvering surface craft,” *International J. Robotics Research*, vol. 29, no. 12, pp. 1461–1474, Oct. 2010.
- [29] A. Bahr, J. J. Leonard, and M. F. Fallon, “Cooperative localization for autonomous underwater vehicles,” *International J. Robotics Research*, vol. 28, no. 6, pp. 714–728, June 2009.
- [30] M. Blain, S. Lemieux, and R. Houde, “Implementation of a ROV navigation system using acoustic/Doppler sensors and Kalman filtering,” in *Proc. 2003 IEEE International Conference on Engineering in the Ocean Environment (OCEANS)*.
- [31] G. Casella and R. L. Berger, *Statistical Inference*, 2nd ed. Duxbury Press, 2001.
- [32] A. Sahai, “Anytime information theory,” Ph.D. dissertation, Massachusetts Institute of Technology, Cambridge, MA, Feb. 2001.
- [33] D. Teneketzis, “On the structure of optimal real-time encoders and decoders in noisy communication,” *IEEE Trans. Inf. Theory*, vol. 52, no. 9, pp. 4017–4035, 2006.
- [34] V. Gupta, “Distributed estimation and control in networked systems,” Ph.D. dissertation, California Institute of Technology, Pasadena, CA, 2006.
- [35] S. M. Ross, *Introduction to Probability Models*, 8th ed. Academic Press, 2003.



Baozhi Chen received his B.S. degree from Beijing University of Posts and Telecommunications, Beijing, China, in 2000. He received his M.S. degree from Columbia University in New York City in 2003. In 2012, he received his Ph.D. degree in Electrical and Computer Engineering at Rutgers, the State University of New Jersey - New Brunswick, under the supervision of Prof. D. Pompili. His research interests lie in underwater communications and networking, communication and coordination of autonomous underwater vehicles, and wireless communications and networking, wireless sensor networks, and wireless body-area networks. He was a co-chair of work-in-progress poster session in ACM WUWNet'12. He also served as technical program committee member in BodyNets'10, GreenNets'11, and GreenNets'12, and as reviewer for ACM and IEEE journals and conferences.



Dario Pompili is an Assoc. Prof. in the Dept. of Electrical and Computer Engineering (ECE) at Rutgers University, where he is the director of the Cyber-Physical Systems Laboratory (CPS Lab) and the site co-director of the NSF Center for Cloud and Autonomic Computing (CAC). He received a Ph.D. in ECE from the Georgia Institute of Technology (GaTech) in 2007. In 2005, he was awarded GaTech BWN-Lab Researcher of the Year. He had previously received his 'Laurea' (integrated B.S./M.S.) and Doctorate degrees in Telecommunications and Systems Engineering from the University of Rome "La Sapienza," Italy, in 2001 and 2004, respectively. In 2011, Dr. Pompili received the NSF CAREER award to design efficient communication solutions for underwater multimedia applications and the Rutgers/ECE Outstanding Young Researcher award. In 2012, he received the ONR Young Investigator Program (YIP) award to develop an uncertainty-aware autonomic mobile computing grid framework as well as the DARPA Young Faculty Award (YFA) to enable complex real-time information processing based on compute-intensive models for operational neuroscience. He is a Senior Member of both the IEEE Communications Society and the ACM.